USING QUASARS AS STANDARD CANDLES: MEASURING

DISTANCES UP TO REDSHIFTS4

A Thesis

presented to

the Faculty ofNatural and Applied Sciences

at Notre Dame University-Louaize

In Partial Fulfillment

of the Requirements for the Degree

Master of Science

---

by

DIANA ISMAIL

February 2019

otre Dame University —Louaize

Facult) ofNatural and Applied Sciences

Department of Physics and Astronomy

We hereb) approve the thesis of

Diana Ismail

Candidate for the degree of Masters in Science

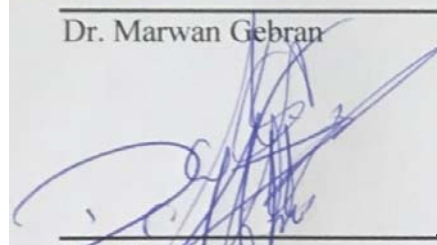Prof. Bassem Sabra   Supervisor

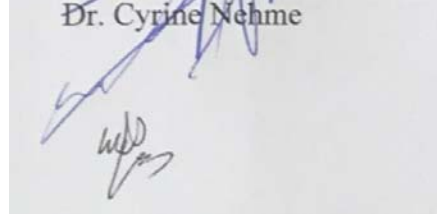Dr. Marwan Gebran   Committee Member, Chair

Dr. Cyrine Nehme   Committee Member

Dr. Wehbeh Farah   Committee Member

Abstract

In this thesis, we have restudied a sample chosen by (Lusso & Risaliti, 2016) consisting of a set of 2,153 unique quasars given by two source catalogues: 3XMM-DR5 (Rosen et al., 2016) and DR7 catalogue (Shen et al., 2011). Quasars serve science in two different ways: 1) Understanding accretion physics by studying the physical mechanism occuring between the disk and cloud corona, and 2) they are good cosmological probes in distance estimation reaching redshifts $\sim$ 7 (Mortlock et al., 2011).

A physical relation has been observed between the optical-UV disk and the X-ray corona through a log-log relation between their respective fluxes (or luminosities). From previous studies, Lusso et al. showed a relation between X-ray and UV luminosities with a dispersion varying between 0.35 to 0.4 dex. That sample was further reduced by eliminating biases including quasars with host galaxy contamination, reddening, X-ray obscured objects and radio loudness in (Lusso & Risaliti, 2016) to reach a dispersion of 0.21-0.24 dex. The least dispersion achieved helps us to better understand the nature of this dispersion and better understand what kind of mechanism is happening between the disk and the corona. In this thesis, the study is performed using a different statistical method, (BCES), presented by Akritas and Bershady to achieve a tight relation with a dispersion of $\sim$0.23 dex.

For now, very little is known about the physics behind the relation, $\alpha_{OX} - \log L_{2500\text{Å}}$. It is a by-product of the luminosity log-log relation. It is further used to calculate luminosity distances (D_L) and build the Hubble Diagram (HD) of quasars' distances versus redshift z. The HD allowed us to constrain the Dark Energy equation of state (EOS) and modify its parameters (Ω_M and Ω_Λ). In this study, we assume a flat ΛCDM model and we obtained $\Omega_M = 0.28 \pm 0.04$ and $\Omega_\Lambda = 0.72$

Keywords: galaxies: AGN - methods: BCES - cosmology: ΛCDM

Acknowledgments

I will dedicate my gratitude to Prof. Bassem in first place as he said a very important statement when I started my Master's studies at NDU. I had my doubts about astrophysics when I first started; I was wondering why are we studying the visible 4% Universe when we have a 96% of unknown science. Dr. Bassem's reply was: Astrophysicists are the feeders of cosmologists. That is the sentence that made me sure that I want to be an astrophysicist some day.

Also, I want to thank all our Dr.'s in the Department of Physics and Astronomy, Dr. Bassem Sabra, Dr. Cyrine Nehme, Dr. Roger Hajjar and Dr. Marwan Gebran, in addition to everyone who taught us at USJ, for all the knowledge you have given us, for the amazing classes we had and for the best observation memories we will keep. It was a great 2 year experience. One I will never get bored of going through all over again!

More thanks go to my colleagues, Jana Sleiman, Nada Moukaddem and Samer Sleiman, for the great times we spent discussing physics and astronomy, for sharing your information with me and for the great help you provided. You taught me a lot. Special thanks go to Jana's sentence: Don't over-complicate physics.

I also want to thank Dr. Elias Kammoun, for the great advice on the topic of quasars. It helped a lot, especially for an amateur trying to understand how to deal with this kind of mysterious science.

Finally, I want to thank my friends and family, mom and dad, for understanding the path I have taken. Thank you for your love and encouragement. Special thanks go to a very dear person in my life, Kamal, for encouraging me and the endless support you have provided me with and the endless talks we had about Astrophysics!

Contents

Appendices

List of Figures

List of Tables

Chapter 1

Introduction

The expansion of the Universe has been a question of interest for the last century when Edwin Hubble introduced a relation between the recessional velocity (v) and distance (d) of astronomical objects, also known as Hubble's Law: $v = H_0 d$, where H_0 is the Hubble constant. The plot showed that the farther the object is, the faster it is moving and thus making our Universe an expanding one (Hubble, 1929). This discovery opened the door to a new topic in cosmology, Dark Energy (DE), that is an unknown form of energy tending to accelerate the expansion of the Universe. But in order to understand the nature and how this energy works, scientists have used different astronomical objects starting with Cepheids and Supernovae 1a (SN1a) to measure distances and recessional speeds of faraway galaxies, as well as different approaches using the cosmic microwave background (CMB), and most recently observed objects known as quasars.

In this thesis, I will base my research on using quasars as standard candles - a method previously introduced by Lusso and Risaliti. As these objects are known to be of high luminosity and extremely bright in the wide electromagnetic spectrum, they can be used to probe vast distances in space and thus we can constrain the equation of state of Dark Energy.

History

For many years, astronomers have been calculating astronomical distances using the luminosities of astronomical objects. In the last two decades, SuperNovae 1a (SN1a) have been used for this purpose along with Cepheid stars. However, Cepheids are limited to small distances, mainly within our Galaxy, and as for SN1a, distances can be reached up to redshifts z~1.5 with high accuracy. Today, even brighter and farther objects are used to calculate even farther distances; Quasars - the most luminous objects, with half million objects detected and spectroscopically confirmed, reaching redshifts z ~ 7 (Mortlock et al., 2011).

How can this be achieved?

There are different approaches in achieving the desired results when studying Quasars:

1. **Studying the variability of fluxes** $L_{2500\text{Å}}$ and $L_{2\text{keV}}$ corresponding to optical-UV and X-ray luminosities, respectively (Dai, Starkman, Stojkovic, Stojkovic, & Weltman, 2012; La Franca, Bianchi, Ponti, Branchini, & Matt, 2014). This allows to find the redshift of these quasars from linear fits to their light curves. The downside is the long duration needed to monitor quasars in order to fit a reasonable light curve (at least 90 days of monitoring).

2. **Reverberation mapping**[1], a method used to measure distances of the Broad Line Region(BLR) clouds [2], and with the help of the distance luminosity relation one can infer luminosities (Watson, Denney, Vestergaard, & Davis, 2011). This method is used up to redshifts z=1, and is extremely difficult on high redshifts. It is also not very reliable due to the little data available that could give a reasonable result.

3. **Baldwin effect**, a method that links luminosities to equivalent widths EW[3] of chosen spectroscopic lines. This method isn't reliable either due to very high dispersion. The inverse correlation between CIV EW and continuum luminosity is known as the "Baldwin Effect". Baldwin showed that the EW of the CIV emission line tends to decrease with increasing continuum luminosity given by the following equation:

$$W_\lambda = \frac{F_{\text{line}}}{F_{\text{c}}} \tag{1.1}$$

where F_{line} is the total line flux and F_c is the continuum level underneath the emission line.

The reason behind this correlation is not clear yet but many assumptions have been made:

- Decrease in ionization parameter (U) with luminosity
- Decrease in covering factor (f) with luminosity
- Disk-inclination effects
- The presence of massive accretion disks in the centers of AGN and quasars. [Netzer, H. (1985). "Quasar discs I. The Baldwin effect"]

4. $L_X - L_{UV}$ **method** used to study the tight relation between Optical-UV and X-ray luminosities and thus infer luminosity distances to build a Hubble Diagram (Lusso & Risaliti, 2016).

---

[1]See further explanation about this method in (Peterson & Horne, 2006)
[2]BLR clouds will be further explained in section 1.1.1
[3]EW, or equivalent width, is the flux ratio that provides strength of a spectral feature
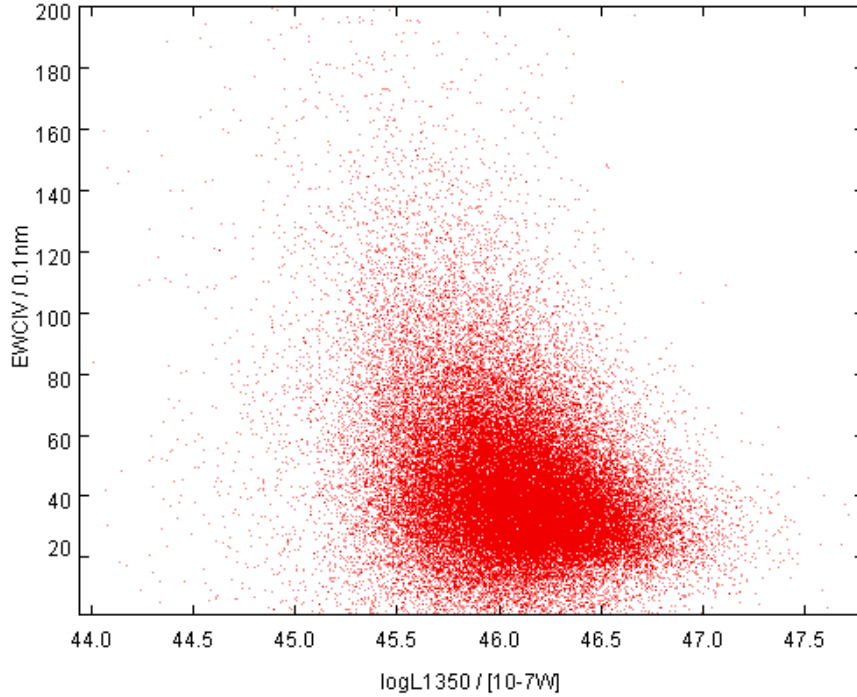
Figure 1.1: Baldwin Effect of the SDSS-DR7 QSO properties catalog containing 105,783 objects. As it appears in this plot that the dispersion is really high and no specific conclusions can be made.

1.1 Previous Literature

One of the first discoveries of the relation between X-ray and Optical-UV luminosities in quasars date back to, almost, 3 decades ago with the first X-ray surveys by Tananbaum et al. with the Einstein X-ray Telescope.

Early Studies

Tananbaum et al. studied the X-ray properties of quasars including the $\frac{1}{L}\frac{L_x}{\text{optical}}$ ratio and α_{ox}, as well as the X-ray time variability. They introduced the ratio α_{ox} defined as:

$$\alpha_{ox} = -\frac{\log \frac{I(v_z)}{I(v_{opt})}}{\log \frac{v_z}{v_{opt}}} \tag{1.2}$$

where for a power-law spectrum, α_{ox} is the energy index or slope connecting the optical with the X-ray band, $I(v)$ is the monochromatic luminosity at a frequency v.

In 1982, Avni and Tananbaum, started studying the dependence of X-ray luminosity of quasars on redshift, optical luminosity and radio luminosity. This lead the way to start studying and constructing physical models of quasars' global properties. In their paper, they found the explicit dependence of L_x on L_o.

Later Studies

Steffen et al. analyzed the correlation between $L_{2500\text{Å}}$, L_{2keV}, α_{ox} and redshift z for optically selected AGNs over wide luminosity and redshift range. The results showed a strong anti-correlation between α_{ox} and $L_{2500\text{Å}}$ with high significance of 13.6σ[4]. Also, an anti-correlation was found between α_{ox} and L_{2keV} but with a lower significance of $\sim 3\sigma$.
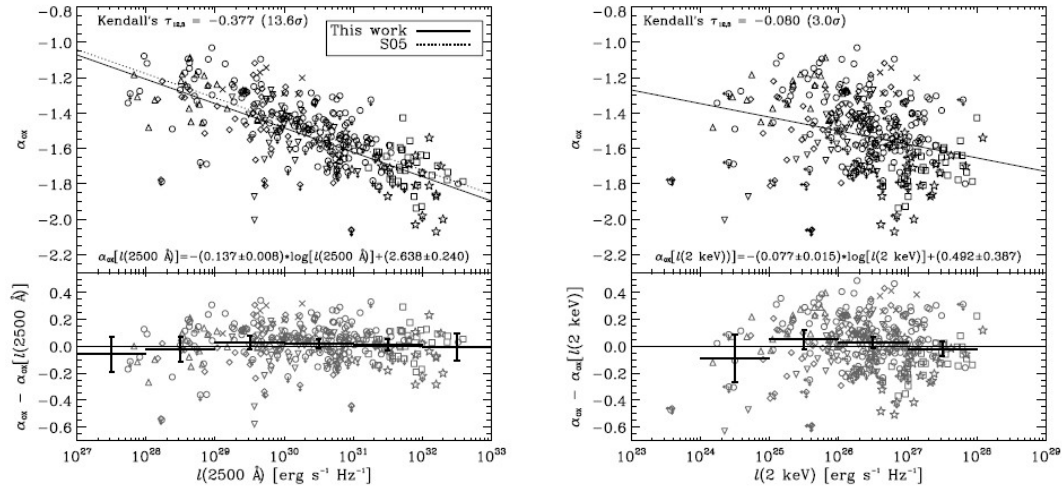
Figure 1.2: (Steffen et al., 2006) results of the relation between α_{ox}, L_{2500A} and L_{2keV}. Left: the anti-correlation between α_{ox} and L_{2500A} with a high significance of 13.6 σ. Right: the anti-correlation between α_{ox} and L_{2keV} with a lower significance 3σ.

Later, Lusso et al., performed a similar study with similar results to those of Steffen et al.. The results are summarized in table 1.1.

Table 1.1: Comparison of significance results between (Steffen et al., 2006) and (Lusso et al., 2010)

Relation	Significance of Full Samples	
	((Steffen et al., 2006))	((Lusso et al., 2010))
$\alpha_{ox} - L_{2500A}$	13.6	21
$\alpha_{ox} - L_{2keV}$	3.0	1.5
$\alpha_{ox} - z$	1.3	<0.1

Recent Studies

The latest research performed to study the properties of quasars was by Lusso & Risaliti. In 2015 and 2016, Risaliti and Lusso; Lusso and Risaliti studied the $L_X - L_{UV}$ relation with more precision by constraining the sample of quasars to least dispersion possible ($\sim$ 0.24 dex). And thus used the following results to further study quasars as cosmological

---

[4]When the significance is higher, that means that α_{ox} and $L_{2500\text{Å}}$ must have an anti-correlation not just by chance.

probes. Bisogni et al. built a Hubble diagram with the best final sample as shown in Figure 1.4.
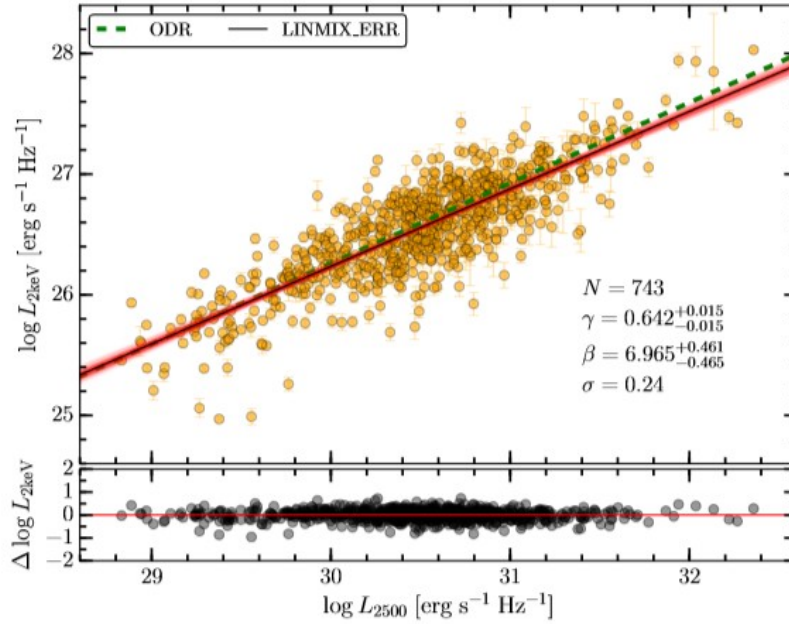
Figure 1.3: (Lusso & Risaliti, 2016) regression using ODR and linmix of the reduced quasars sample (containing 743 objects) for the monochromatic rest-frame luminosities L_{2keV} vs L_{2500A}. In this plot it is shown that the dispersion has went down to 0.24 dex.

1.2 Algorithm of this work

The study starts with choosing a sample that can serve the aim of obtaining an enough constrained sample that has enough quasars to perform statistical plots. I first performed a cross-match between SDSS-DR7 and 3XMM-DR5 catalogues, that allowed me to obtain a reduced data sample containing $\sim 2,000$ quasars having X-ray and Optical-UV fluxes as introduced by the two catalogues which will be discussed in Chapter 3. This sample was further reduced to 730 objects that helped finding the tight relation between two fluxes as well as two luminosities, 2500A and 2keV, that represent the frequencies released by the accretion disk and the corona, respectively. The relation is obtained by fitting a linear regression in log-log space introduced by a statistical model for linear fitting BCES: Bivariate Correlated Errors and intrinsic Scatter. The following will be discussed in Chapter 4.

A linear relation is adopted in the form of $y = ax + b$ to reach the least dispersion possible after removing biases from the sample. The linear relation results in a quantitative relation of fluxes and luminosities and it might explain more about the physical mechanism occurring between the disk and corona. Also it allows us to understand the
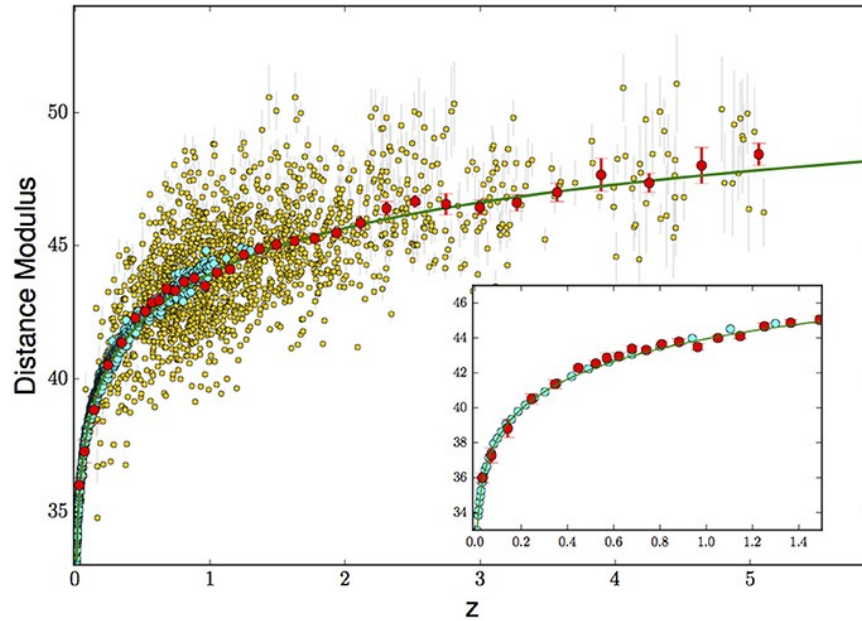
Figure 1.4: A joint Hubble Diagram of Quasars and SN1a presented by (Bisogni et al., 2018) showing the fit of the distance modulus as a function of redshift z. Th light blue dots are SN1a, the yellow dots represent the entire quasar sample and the red dots are the redshift bins of quasars. The plotted curve represents the ΛCDM model fit assuming $H_0 = 70 km^{-1}Mpc^{-1}$, $\Omega_M = 0.3$ and $\Omega_\Lambda = 0.7$.

reason behind the high dispersion that has been observed throughout previous studies. The results of this fit will be shown in Chapter 5.

After finding the relation, we're ready to further go into deducing the luminosity distance, discussed in Chapter 6, which will be achieved by fitting the $\alpha_{ox} - L_{2500\text{Å}}$ relation, build a Hubble diagram of the distance as a function of redshift and obtain the parameters of the Dark Energy equation of state Ω_M and Ω_Λ.

Finally, the results of this study are discussed in Chapter 7 with comparison to previous work done on this topic.

Chapter 2

Quasars, Standard Candles and Dark Energy

The first quasars were discovered in the late 1950s as radio sources in all-sky radio surveys. They were first noted as radio sources with no corresponding visible object and have also shown to have a very small angular size.

The term "quasar" was given by the astrophysicist Hong-Yee Chiu in May 1964 to describe these puzzling objects:

So far, the clumsily long name 'quasi-stellar radio sources' is used to describe these objects. Because the nature of these objects is entirely unknown, it is hard to prepare a short, appropriate nomenclature for them so that their essential properties are obvious from their name. For convenience, the abbreviated form 'quasar' will be used throughout this paper.

As the name says, Quasars are known to be quasi-stellar radio objects. First recognized as stars, yet with extremely high luminosities and not fitting the blackbody diagram as a star usually does. The extremely high luminosities of these objects implied that it was the aftermath of physical extremes that were not found elsewhere in the nearby universe. Zeldovich and Novikov, (Zeldovich & Novikov, 1964), suggested that massive blackholes might be involved. In addition to that, the high luminosities also imply that they might serve as important cosmological probes due to their high redshifts.

These extreme properties provided continuous studies in order to detect and analyze the physics behind them. Until this day, the number of detected QSO objects has reached hundreds of thousands with redshifts reaching $z \sim 7$(Mortlock et al., 2011).

2.1 Properties and Anatomy of Quasars

Schmidt had studied a sufficient number of quasars by the late 1964 and defined the following properties (Peterson, 1997):

- Star-like objects identified with radio sources.

- Time-variable continuum flux.

- Large UV flux

- Broad emission lines

- Large redshifts

It is commonly thought that a quasar is powered by a supermassive black-hole at the center of a galaxy as suggested by Zeldovich and Novikov. As matter infalls onto this black-hole, an accretion disk is created. And as more matter continues to fall, it gets highly heated by frictional and gravitational effects releasing huge amounts of energy. Ionization cones extend outward as funnels of ionizing radiation that escape from above and below the torus, radiating clouds of gas within the host galaxy which glow. Also present are the two radio jets.

The clouds closest to the accretion disc have broad emission lines and form the broad-line region (BLR). Broad spectral lines means that the narrow peeks normally associated with spectra have been broadened and the most obvious mechanism in this case is Doppler broadening. High-speed motions in these clouds will broaden the range of wavelengths over which the emission peek is visible. The broadening seen in the BLR corresponds to cloud velocities of about 10 000 km/s.

Further away (50-100 pc) in the ionisation cone, are clouds of the narrow-line region (NLR) where velocities are lower and so the emission lines broadened less, although the peeks are still broad compared to those seen in non-AGN galaxies and correspond to velocities of several hundred km/s. Further out still is the extended narrow-line region (ENLR).

As illustrated in Fig. 2.1, the anatomy of an AGN clearly shows each part described in the previous paragraphs.

2.2 Standard Candles

What are Standard Candles?
Think of it as if you're walking on a straight road where at the sidewalk there are street lamps aligned along your path. If you look at the lamps' brightness assuming that they all shine with the same strength, you can easily understand which is closer and which is farther, and using this information (apparent brightness, i.e how faint or strong the light is and strength, i.e luminosity) one can estimate at what distances these lamps lie. The same concept applies to how astronomers study cosmological distances.
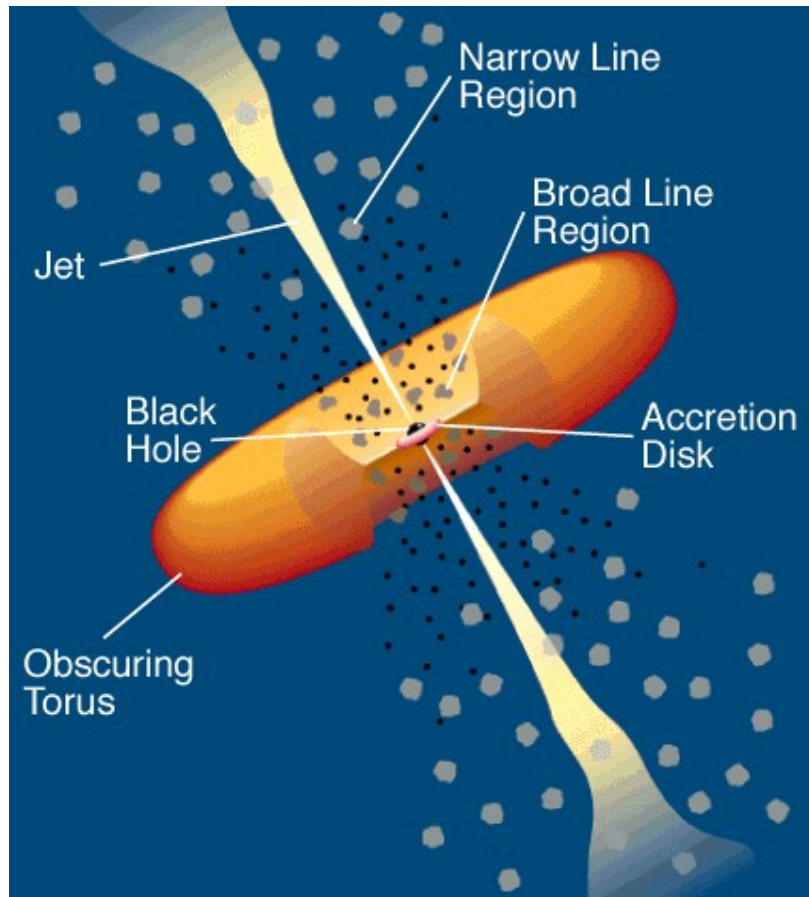
Figure 2.1: Basic model of the structure surrounding the nuclear region, as illustrated by Urry and Padovani.

$$ApparentBrightness = \frac{Luminosity(orstrength)}{4\pi(distance)^2}$$

SuperNova 1a (SN1a)

Type 1a SuperNova have been widely used for the last couple of decades in studying the expansion of the Universe - and that was an evolutionary step in this field.

The fit below, Figure 2.3, describes the change of the distance modulus[1] as a function of redshift z. Betoule et al. fit several sets of SN1a data starting from low redshift SN, ending with data achieved by the Hubble Space Telescope (HST). There are several conclusions that can be drawn from this figure:

1. The distance is increasing in a specific pattern as redshift increases, telling us that as we look farther, we notice that distances tend to increase, and thus we can conclude there is some "force" leading to this expansion

---

[1]distance modulus will be further discussed in section 6.3
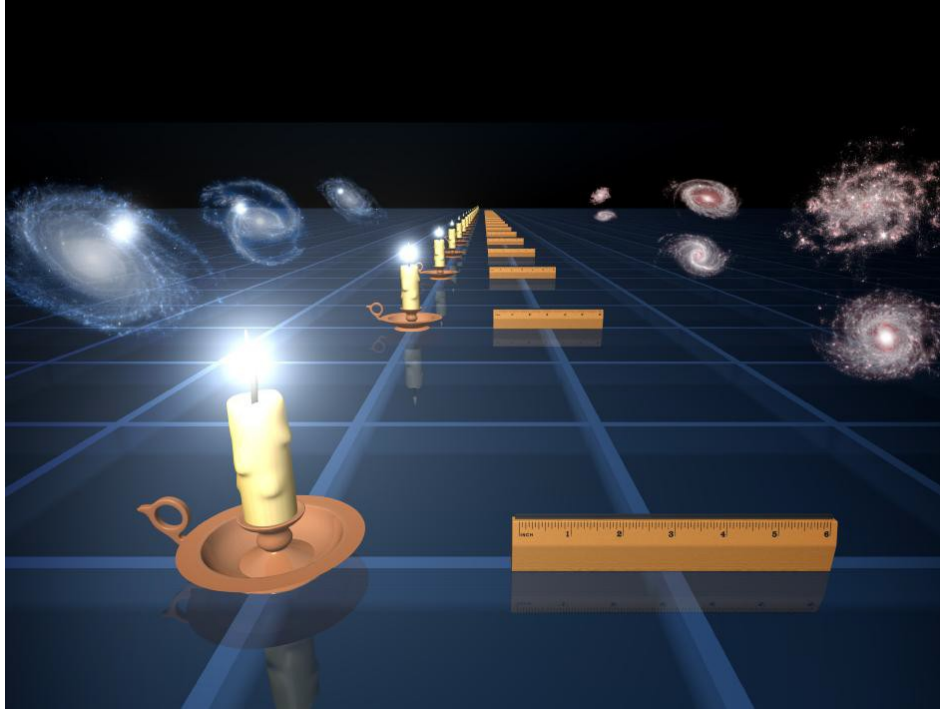
Figure 2.2: A simplification of the concept of "Standard Candles". From the strength of the candles, we can conclude how far it is from us. The same works for astronomical objects if they have a known, or standard, strength.
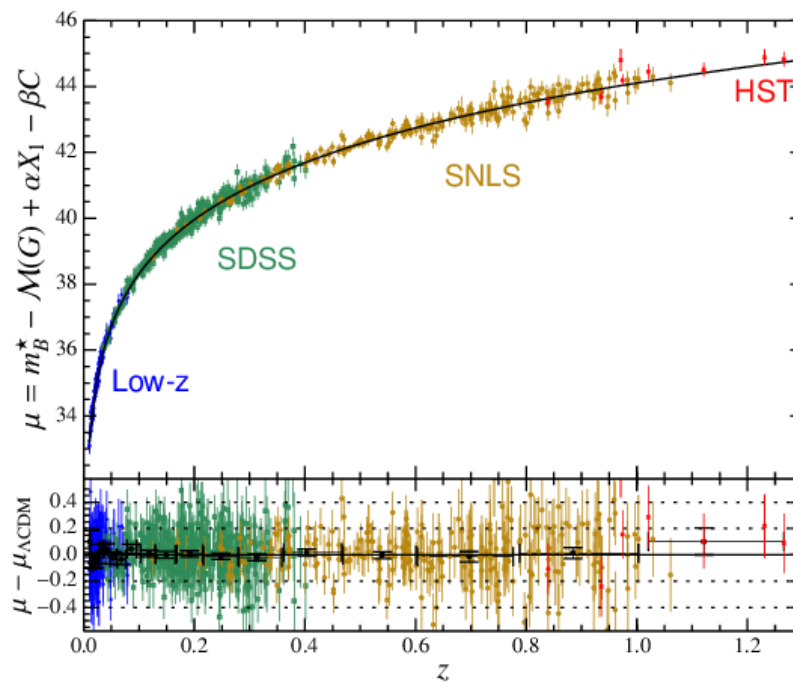
Figure 2.3: Hubble Diagram of SN1a presented by Betoule et al. showing a joint fit of the distance modulus as a function of redshift z

2. A very important observation we should notice is that the fit is up to redshift ~ 1.3. That is a problem for astronomers when studying cosmological models. In reality, the fit is over a very small part of the entire range, and since SN1a data at redshifts >1.7 isn't available due to their faint luminosities at large distances, one cannot extend it to higher redshifts

3. Astronomers should wait for a supernova to occur and they would have a short window of time to make their observations.

Thus, we can conclude that SN1a were very good estimators for observational cosmologists at relating low redshifts, but due to their faint luminosities at high redshifts and low occurrence, one should find a better estimator to go for higher redshifts and test for the validity of the cosmological models used.

2.3   Dark Energy

As astronomers went into deep observations of the universe, going outside our Galaxy and observing distant ones, they noticed that everything was actually moving away from us (Hubble, 1929), something we also call the redshift of an object. That is when the concept of expansion of the universe was brought in. Of course, this is not the end, since there should be a force moving everything away from us, this is now known as **Dark Energy**[2] - an unknown force that is performing this job.

Moreover, in 1998, while Riess et al. were studying SN1a, they noticed that not only was the universe expanding, but it was accelerating in its expansion. So now, dark energy is known as the mysterious force accelerating the expansion of the universe allowing everything to move faster and faster away with time. And in order to understand more about it, many fields are contributing to study this phenomenon; mostly cosmologists and observational cosmologists. The cosmological model that will be adopted in this study is the flat-ΛCDM model that allows us to apply Newtonian mechanics in the local Universe.

2.4   The contribution of Quasars

Quasars have given, not only the chance to study their own physical phenomena, but also the chance to use them as mid-men for studying the global picture, the cosmos. As mentioned before, studying the quasars' luminosities, we are able to deduce distances in space reaching high redshifts (Lusso & Risaliti, 2016).

---

[2]Dark Energy, DE, leads to the expansion of the universe
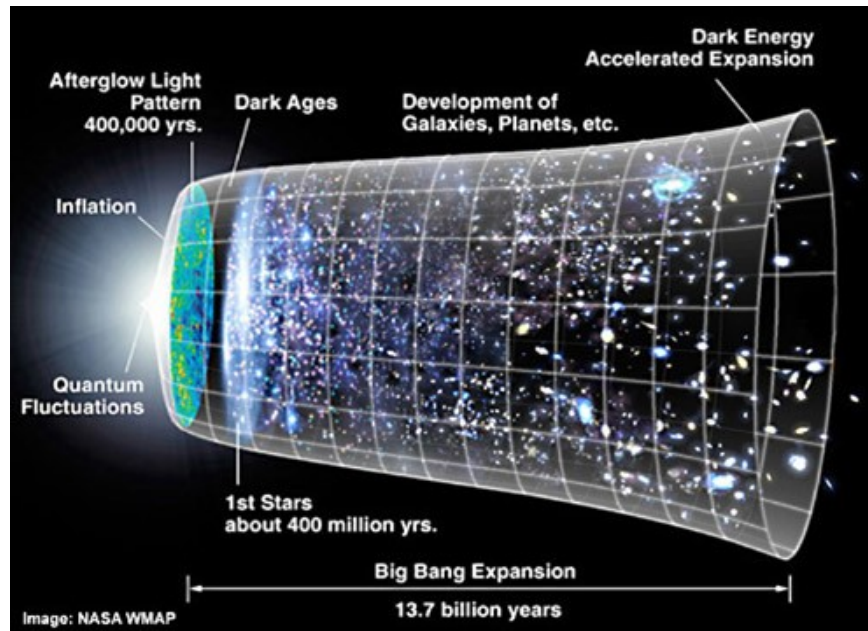
Figure 2.4: Dark energy responsible for the accelerated expansion of the universe, and most fundamental to understand the evolution of it after the Big Bang. Photo taken by NASA WMAP

Since too little is known about quasars, there are many physical phenomena researchers are trying to explain. One of what we are interested in is the physical relation between the accretion disk (very close to the black hole) and the corona surrounding the BH.

From previous studies, this relation is known as the $L_X - L_{UV}$ (Lusso et al., 2010) which links the monochromatic luminosities of the X-ray corona and the UV disk. The following will be discussed below.

2.4.1   X-ray - UV Relation in Quasars

For more than 30 years, observational evidence showed the existence of a link between the X-ray corona (L_X at 2keV) and the accretion disk UV emission (L_{UV} at $2500\mathring{A}$) in AGN.

In this study, the method used is the non-linear tight relation between UV and X-ray luminosities[3]. This method is recent and very well studied by (Lusso & Risaliti, 2016). The first discovery was done by Avni, Soltan, Tananbaum, and Zamorani. Now it's very known, using this tight log-log relation, that the ratio between X-ray and UV emission in Quasars decreases with luminosity. That means, more optically luminous quasars are relatively less luminous in X-rays. That could be due to many different factors including: enhanced X-ray emission associated with the jets of radio-loud AGN; X-ray absorption

---

[3]The relation between luminosities is non-linear, so it was transformed into a log-log relation to get linearity

associated with the UV Broad Absorption Line (BAL) outflows; intrinsic X-ray weak-ness; UV and X-ray variability, and non-simultaneity of UV and X-ray observations. Once the ratio between X-ray and UV luminosities is achieved one can infer distances and build a Hubble Diagram that is further explained in Chapter:6.

2.4.2 Luminosities Used

Quasars emit in all frequencies of the electromagnetic spectrum, i.e radio, infrared, vis-ible, ultra-violet and X-rays. Each part of the quasar is responsible for part of the emitted radiation.

As shown previously in the anatomy of Quasars, in the inner region of the accretion disk, very close to the SMBH, the peak of the emission is in the UV, particularly at $2500\mathring{A}$.

As for X-ray emission from the corona, it is due to the inverse compton mechanism of the up-scattered photons coming from the accretion disk. The corona is just a cloud with hot electrons surrounding the SMBH with unknown shape and exact position. But from variability studies in X-rays, it was shown that the corona is a few gravitational radii and not too far from the BH. So the reprocessed electrons from the accretion disk emit in X-rays, particularily at 2 keV (Avni et al., 1980).

The linear relation between UV and X-ray components has the following form:

$$logL_X = \gamma logL_{UV} + \beta$$

$$logF_X = \gamma logF_{UV} + \beta$$

This relation tells us that there should be a strong link between the chosen lumi-nosities, because, suppose there isn't, if we consider the thermal energy from this cloud of electrons to be a certain given, the cloud will cool down very rapidly if there were no interaction with the energy transported from the accretion disk, whereas in reality we can see that the relation is stable at the inner accretion disk (given by a power law of X-rays). The energy lost from the inner disk is transported into the hot corona thus emitting in the X-rays. This relation is not seen in the wings of the disk (optical), that's why we use the inner disk for the following study.

2.4.3 Choice of the specific values: 2500 Angstrom and 2 keV

The first question that comes to mind when reading quasars studies is the choice of 2500 Angstrom and 2 keV fluxes of the UV and X-ray radiation, respectively. To answer this question, all we need is simplicity. Since we are studying extremely complex objects that are pretty much far from our Galaxy, they undergo Galactic absorption, reddening, host

galaxy contamination and more. It was historically easy to study the following fluxes back in the 1980's (Avni et al., 1980).

Nowadays, we still use those values because they are observationally convenient. The 2500$\mathring{A}$ (UV) is not an overly red wavelength so it's not contaminated by the host galaxy and it's not too blue to be contaminated by neutral Hydrogen found in the host galaxies' interstellar medium. As for the 2 keV flux, it's very convenient too since it's high enough to be insensitive to Galactic absorption and X-ray telescopes have the highest sensitivity in that range.

Chapter 3

Quasar Sample

The data sample used for this study was chosen by cross-matching two catalogues: SDSS-DR7, catalog of quasars properties presented by Shen et al., with 3XMM-DR5, the third generation catalogue of serendipitous X-ray sources presented by Rosen et al. leaving us with 2,153 unique quasars.

Not forgetting about the aim of achieving the "best" sample for the study in order to understand to what degree the scatter on the $L_{2500\text{Å}}$-L_{2keV} relation varies, the selection criteria will be explained.

3.1   The Catalogues Chosen

To start off, in order to achieve the desired data sample, TOPCAT software was used (Taylor, 2005). TOPCAT is a Virtual Observatory, an astronomical (can be used for other purposes) interactive graphical viewer and editor for tabular data. It offers astronomers an easy way to deal with analysis and manipulation of source catalogues and other tables. It also facilitates fast access to large data sets, edit them and view plots of quantities against each other (2D/3D plots, histograms..). Using its features, I was able to cross-match and clean the catalogues.

The Shen et al. catalog of quasar properties is made of 105,783 spectroscopically confirmed broad-lined quasars. From this catalog, BAL[1] (Broad Absorption Line) and Radio Loud[2] (Radio Loudness = $F_{6cm}/F_{2500\text{Å}}$ >= 10 (Kellermann, Sramek, Schmidt, Shaffer, & Green, 1989)) quasars were excluded. In TOPCAT, one can add row subsets by including a statement of their choice. In our case, to exclude the above the statement used is: "BAL = 0 and RL < 10" (Kellermann et al., 1989). Then three more quasars were excluded from the SDSS-DR7 catalogue flagged as BAL's by Gibson et al..

---

[1] BALs are known to be X-ray obscured(Green & Mathur, 1995; Gallagher, Brandt, Sambruna, Mathur, & Yamasaki, 1999; Brandt, Laor, & Wills, 2000), and are not included in previous studies of optically selected samples because they cause artificial steepening of the $L_{2keV} - L_{2500A}$ relation

[2] Radio Loud quasars have an additional jet-lined X-ray component

The Rosen et al. 3XMM-DR5 catalog is the third generation catalogue of serendipitous X-ray sources and contains 565,962 X-ray source detections with 396,910 unique X-ray sources, i.e with only 1 observation. Cuts have also been performed to this catalog in order to define a "clean" sample by choosing low level of spurious detections and low background levels. In TOPCAT, this was implemented by the following statement: "SUM _-FLAG<3 and HIGH _-BACKGROUND = 0".

The results of the following cuts was cross-matched in TOPCAT with criteria including sky algorithm and 3 arcsec max error to provide optical classification and spectroscopic redshift for all objects (Lusso & Risaliti, 2016). The net sky coverage is ~877 deg^2 with a net exposure time >= 1ks for each source. The remaining sample after these cuts is made of 3304 XMM observations (2155 unique sources and 470 with 2 or more observations). For sources with multiple observations, the one with the longest exposure time has been chosen. This choice is the most appropriate in order to minimize the Eddington Bias[3] due to flux limit of each observation.

3.2   Reducing host-galaxy and reddening contamination

In order to minimize reddening and host-galaxy contamination, the approach applied here is similar to that of Risaliti and Lusso. It is important to remove dust extinction in order to reduce bias on further results. Dust extinction affects the 2500Å flux more than the 2keV one even considering a small amount of dust. If we assume a column density of 10^{22} cm^{-2}, the UV flux would be reduced by a factor of two, while the 2keV flux will nearly stay unaffected (Lusso & Risaliti, 2016).

To reduce the effects of dust reddening on our sample, we plot Γ_1 slope of the spectral energy distribution (SED) log(v) - log(vFv) power-law in the 0.3-1 μm rest frame range and Γ_2 in the 1,450-3,000 $\mathring{A}$ (rest frame) range of each object - both Γ_1 and Γ_2 values are given in the quasar catalog of Shen et al.. The $\Gamma_1 - \Gamma_2$ plot is shown in Fig 2.2. The considered minimization used is an extinction of E(B-V)$\leq$0.1 in order to constrain the data to the least reddening in the sample - these sources are highlighted in black within the circle - ending up with 730 objects[4].

---

[3]Eddington Bias is what you get because of statistical fluctuations in a measurement (Eddington, 1913)

[4]Assuming a lower extinction value will constrain the sample in a way that not too much objects are left for later statistical analysis
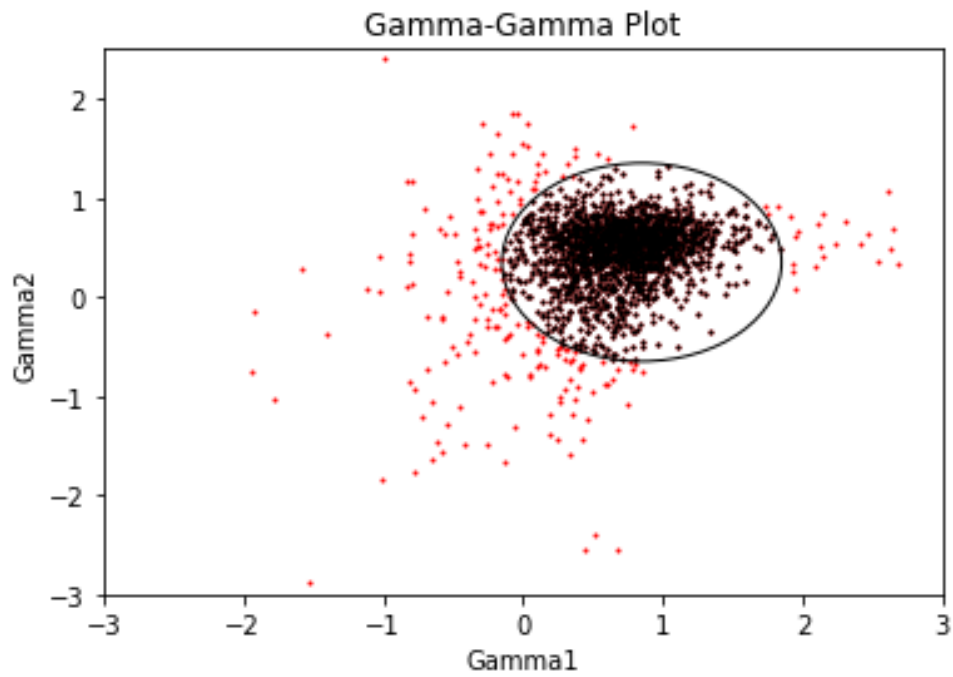
Figure 3.1: $\Gamma_1 - \Gamma_2$ plot of the quasar sample after reduction (S/N>5 and $1.9 \leq \Gamma_X \leq 2.8$ containing 730 objects. In this plot, the minimization used is E(B-V)$\leq$0.1 where the least reddening is to be considered

.

Chapter 4

Statistical Approach

The relation $L_{2500\text{Å}} - L_{2\text{keV}}$ provides an insight on the physical mechanism and it's important to find a relation that can lead to a physical explanation. The simplest form of relations is a linear one. Optical-UV photons from the accretion disk (paramertrized by $L_{2500\text{Å}}$) are Compton up-scattered by hot electrons and lead to the formation of a power law spectrum in the X-rays (parametrized by $L_{2\text{keV}}$) accompanied by a high energy cut-off at the electrons temperature.

For the following study, I adopted an Ordinary Least Square linear regression with errors on both X and Y variables. Where X is the luminosity/flux at 2500Å and Y is the luminosity/flux at 2 keV.

4.1 Linear Regression

Linear regression is one of the most common and used statistical approaches used in astronomical data analysis due to its simplicity, especially when we are working with two variables, one being dependent on the other (with the second one being an independent variable).

The result of such a regression is a simple equation $y_i = ax_i + b$ relating x (the independent variable) with y (the dependent variable). In astronomy, linear regression is characterized by intrinsic scatter about the regression line and measurement error in both the dependent and independent variables which adds a constant E to the linear equation

$$y_i = ax_i + b + E$$

where E is the intrinsic scatter, an unknown, and is treated as a model constant. And due to the presence of intrinsic scatter and measurement error on both variables, it is important to account for them while performing a regression.

Intrinsic Scatter The source of intrinsic scatter is variations in the physical properties of astronomical sources that are not completely captured by the variables included in

the regression.

Measurement Error Also known as observational error, is the difference between the actual value of the objects "value of interest" and the one measured by us. This could be due to the biases caused by the instrument used and calibration. Also many of these errors come due to the fact that along the line of sight, a lot of cosmic dust decalibrates the objects original light.

4.2 BCES: Linear Regression for Astronomincal Data with Measurement Errors and Intrinsic Scatter

On the contrary to Lusso and Risaliti where they used linmix[1] for linear regression, I have used a less complicated method presented by Akritas and Bershady. It is a simple linear regression method performed on observed astronomical data to account for measurement errors in their linear regression. Due to the fact that the data is observed, correlations exhibit intrinsic and measurement error for which we should account while trying to find a correlation.

The BCES (Bivariate Correlated Errors and Intrinsic Scatter) estimator has its pros and cons. As mentioned, this method takes into account measurement error on both variables x and y as well as intrinsic scatter, unlike other methods like the Weighted Least Squares (WLS), which considers measurement error only on one variable with no intrinsic scatter. Linmix, like BCES with the mentioned above. But Linmix gives the advantage to work with it when the data is censored[2] In our study, the sample consists of 2,153 quasars which have X-ray and UV data (no censored data), thus the chosen regression model follows that presented by Akritas and Bershady and the python package worked out by Nemmen et al..

Statistical Model

BCES has the following model:

$$y_i = \alpha x_i + \beta + E_i \tag{4.1}$$

where $E_i \sim N(0, \sigma^2)$, the intrinsic scatter with zero mean and finite variance. Also, the intercept is given by

$$\beta = \frac{cov(x, y) - \sigma_{xy}}{var(x) - \sigma_x^2}$$

and slope

$$\alpha = \bar{y} - \beta \bar{x}$$

---

[1]Linmix is a hierarchical Bayesian model for fitting a straight line to data with errors in both the x and y directions. This model is described in detail by Kelly

[2]Lusso and Risaliti used linmix in the first sample where X-ray data was censored.

where cov(x,y) is the covariance between the independent x and dependent y variables, σ_{xy} is the dispersion of the respective variables, var(x) the variance of the independent x variable and σ_x the standard deviation of x.

In addition to the module presented by Nemmen et al. in their python package, we included intrinsic dispersion by hand since it is not integrated in the code. We used a method suggested by Tremaine et al. and used by Sabra, Saliba, Akl, and Chahine given by the following equation:

$$\chi^2 = \Sigma_{i=0}^n \frac{(y_i - \alpha x_i - \beta)^2 + \alpha_{\mathrm{Xerr}}^2}{\sigma_X^2 - \sigma_X err^2 + \sigma_{int}^2}$$

with σ_X being the standard deviation of the independent variable X, σ_{Xerr} the variance of its error, and σ_{int} denoting the intrinsic dispersion.

In order to estimate the value of the intrinsic dispersion σ_{int}, one should minimize the value of $\frac{\chi^2}{dof}$. This fraction should approach unity, where dof are the degrees of freedom of the system - the value of variables subtracted from the number of objects. The intrinsic dispersion, as stated before, tells us more about the variation happening in the system itself, excluding measurement errors affecting the system. This means that if we have a good estimate of measurement uncertainties on this system, σ_{Xerr}, the ratio $\frac{\chi^2}{dof}$ will approach unity for a certain value of σ_{int}.

4.3   Python package

The regression method presented by Akritas and Bershady has a python package BCES worked out by Nemmen et al..

Module

A class to perform linear regression of y on x when there are measurement errors in both variables is given as

Usage

import bces.bces a,b,aerr,berr,covab=bces.bces.bces(x,xerr,y,yerr,cov)

Arguments:

- x,y : 1D data arrays

- xerr,yerr: measurement errors affecting x and y, 1D arrays

- cov : covariance between the measurement errors, 1D array

output:

- a,b : best-fit parameters a,b of the linear regression such that $y = Ax + B$.

- aerr,berr : the standard deviations in a,b

- covab : the covariance between a and b (e.g. for plotting confidence bands)

Chapter 5

Results and Further Constraints

In Chapter 4, I introduced the statistical method used to calculate the relation between the UV and X-ray luminosities. In this Chapter, I will present the results of the BCES method, starting with the reduced sample containing 730 objects that was achieved by previously mentioned constrictions in Chapter 3. I will wrap up this chapter by a detailed explanation and analysis of the results upon each assumption.

5.1   X-ray - UV Relation Fits

Determination of γ, β, and σ

As mentioned in the previous chapters, we want to examine the relation between the UV disk and X-ray corona, to better understand what physics lies behind this relation. As far as we could get is a linear relation between the log of the X-ray and UV fluxes. And with time, researchers are trying to clean out the sample to leave data unbiased by measurement error in order to reach a minimum intrinsic dispersion that could better explain what mechanisms might be occurring in the disk-corona system.

Lusso and Risaliti previously studied the relation starting with the main sample containing 2,153 objects, leading to a high dispersion of $\sigma \sim$ 0.4 dex. Apply further constraints on the given sample in order to get the least dispersion possible, yet keeping in mind that too few objects is a bias to the study as well[1]. Thus the sample was reduced significantly to yield a dispersion $\sigma = 0.24$ dex.

Lusso and Risaliti sample was reduced from 2,153 to 1,898 objects where host galaxy contaminated and dust reddened quasars were eliminated, as mentioned in section 3.2, keeping those with the least contamination by assuming an extinction E(B-V) ≤ 0.1[2]. Further constraints included objects with higher S/N ratio (first taking S/N > 3, then S/N > 5). And last, the sample was cleaned off quasars with X-ray absorption[3], taking

---

[1]When studying SN1a in higher redshifts, the number of objects were fewer, thus they can't be taken into consideration when making these kinds of plots

[2]As seen in Figure 3.1, data within the black circle

[3]Some soft X-ray fluxes contain absorption

into consideration to keep the sample with a photon index $1.9 \leq \Gamma_X \leq 2.8$. This final sample contains 743 objects and reduced the dispersion down to $\sigma = 0.24$ dex. The results of these reductions are shown in Table 5.1.

In our study, we performed the same reductions applied by Lusso and Risaliti, ending up with sample of 730 quasars with signal-to-noise ratio > 5, a photon index (Γ_X) ranging between 1.9 and 2.8, and extinction E(B-V) ≤ 0.1.

We have adopted two relations:

1. $\log L_X - \log L_{UV}$ relation of the UV and X-ray luminosities

2. and the $\log F_X - \log F_{UV}$ relation of the UV and X-ray fluxes

since luminosities are distance dependent, it is important to eliminate that factor from the equation. For that reason, I will be plotting fluxes for the same relations that (Lusso & Risaliti, 2016) have previously used.

The variables are given by X: $L_{2500\text{Å}}$ the independent variable and Y: $L_{2\text{keV}}$ the dependent variable as mentioned before. As for the measurement error, it is only provided for the X-ray luminosities in the sample, but wasn't provided by the SDSS catalogue for the UV luminosities. Previously, Lusso and Risaliti adopted a 2% error on the UV luminosity stating that it's a good approximation when the average bolometric luminosity is around 3%[4]. But, if one calculates the average uncertainty on the bolometric luminosity for the cleaned sample (containing ~730 objects), it turns out to be much less than 3% (~0.022% according to my calculations), and a maximum error of 0.5%. I have also calculated the average uncertainty on the X-ray luminosities, which is 0.23%. All three uncertainties were used to check for the different results achieved.

Our results are summarized in tables 5.1 and 5.2 of both fluxes and luminosities relations. The results show that from the $\log L_X - \log L_{UV}$ regression, the slope varies between 0.635 and 0.685 (± 0.016), but when it comes to the $\log F_X - \log F_{UV}$ relation, the variation becomes bigger - between 0.65 and 0.75 (± 0.045). The results are also shown in figures 5.1 and 5.2 with the fits being within the confidence band of slopes. Despite that, the results in both cases agree with the prediction set in early studies where optically bright AGN emit less X-rays than optically faint AGN and thus a correlation exists between the UV disk and X-ray corona.

More importantly, the intrinsic dispersion achieved in this study is as low as 0.24 dex agreeing with the results of Lusso and Risaliti when plotting the log-log plot of luminosities, yet it is still high in the log-log flux relation (0.36 dex). According to Lusso and Risaliti, the physical dispersion should be less than 0.21 dex and the additional dispersion is due to the measurement uncertainties we didn't yet account for. In addition

---

[4]The uncertainty on the bolometric luminosity is provided by the SDSS-DR7 catalog.

to that, the variability of X-ray flux accounts to **30%** (0.063 dex) of the dispersion. Another 0.147 dex are left out without explanation- this could be another statistical dispersion, or a physical mechanism causing this change. This matter will be addressed in more detail in later studies.
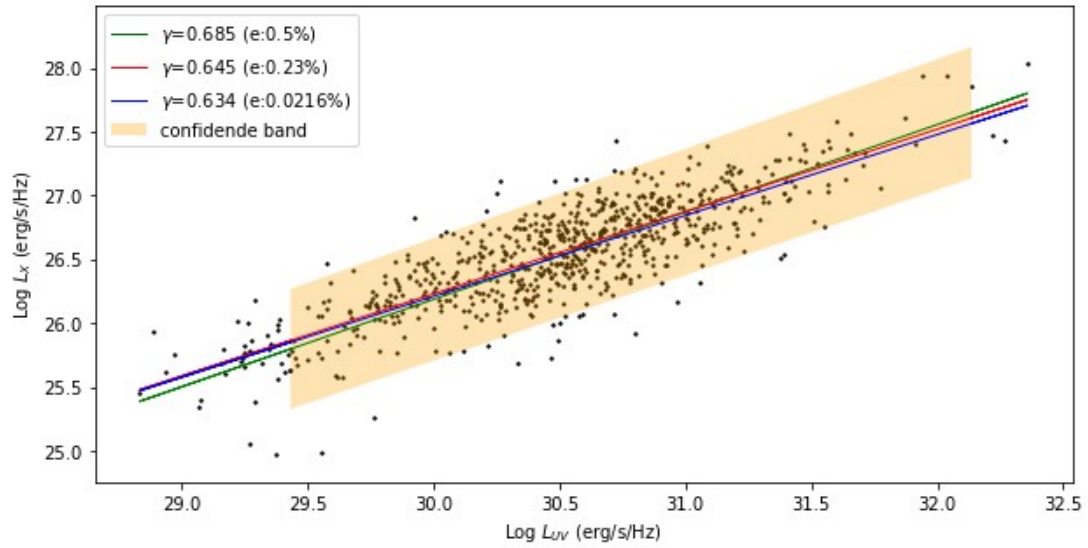
Figure 5.1: Rest-frame monochromatic luminosities relation
.
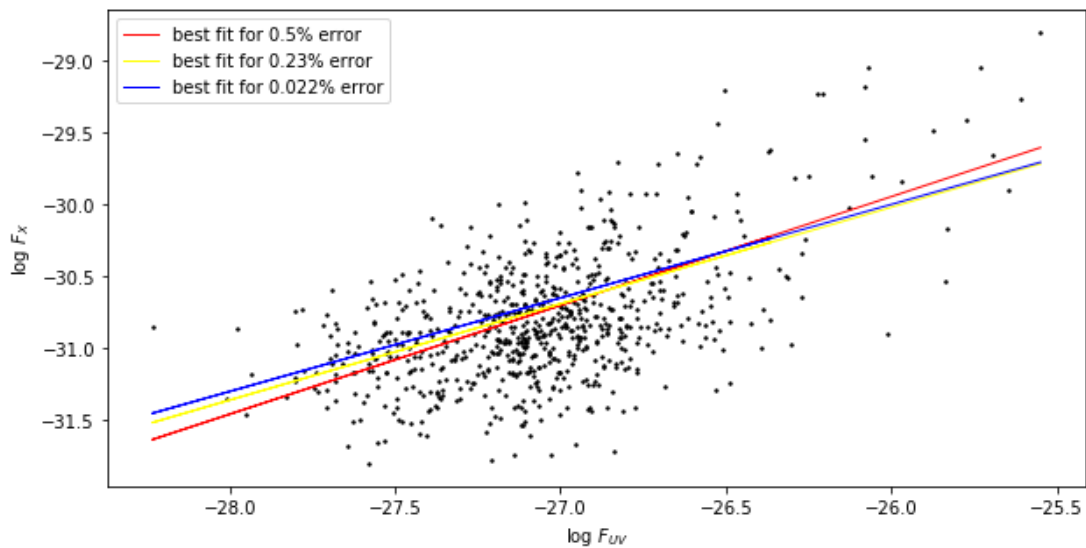
Figure 5.2: Rest-frame monochromatic fluxes relation.
.

Table 5.1: Results of the $\log L_X - \log L_{UV}$ plot with different error values on the UV luminosity with their respective intrinsic dispersion values summarized in this table

Lusso and Risaliti Sample	$error_{UV}$	slope γ	interceptβ	σ_{int} (dex)	N_{total}
Main	2%	0.583 ± 0.014	$8.697^{+0.415}_{-0.412}$	0.42	2153
E(B-V)≤0.1	2%	0.596 ± 0.016	$8.279^{+0.460}_{-0.478}$	0.40	1898
E(B-V)≤0.1 - S/N>3	2%	0.596 ± 0.015	$8.279^{+0.462}_{-0.469}$	0.40	1889
E(B-V)≤0.1 - S/N>5	2%	0.589 ± 0.015	$8.539^{+0.456}_{-0.465}$	0.35	1683
E(B-V)≤0.1 - S/N>5 - 1.6≤Γ_X ≤2.8	2%	0.596 ± 0.014	$8.392^{+0.415}_{-0.398}$	0.28	1298
E(B-V)≤0.1 - S/N>5 - 1.9≤Γ_X ≤2.8	2%	0.642 ± 0.015	$6.965^{+0.461}_{-0.465}$	0.24	743
Our Sample	$error_{UV}$	slope γ	interceptβ	σ_{int} (dex)	N_{total}
E(B-V)≤0.1 - S/N>5 - 1.9≤Γ_X ≤2.8	0.022%	0.635 ± 0.016	7.19 ± 0.49	0.23	730
E(B-V)≤0.1 - S/N>5 - 1.9≤Γ_X ≤2.8	0.23%	0.645 ± 0.016	6.884 ± 0.5	0.23	730
E(B-V)≤0.1 - S/N>5 - 1.9≤Γ_X ≤2.8	0.5%	0.685 ± 0.017	5.635 ± 0.53	0.24	730

Table 5.2: Results of the $\log F_X - \log F_{UV}$ plot with different error values on the UV fluxes with their respective intrinsic dispersion values summarized in this table

Our sample	$error_{UV}$	slope γ	intercept β	σ_{int} (dex)	N_{total}
E(B-V)≤0.1 - S/N>5 - 1.9≤Γ_X ≤2.8	0.5%	0.75 ± 0.04	-10.3 ± 1.08	0.36	730
E(B-V)≤0.1 - S/N>5 - 1.9≤Γ_X ≤2.8	0.23%	0.67 ± 0.048	-12.6 ± 1.3	0.35	730
E(B-V)≤0.1 - S/N>5 - 1.9≤Γ_X ≤2.8	0.022%	0.65 ± 0.047	-13.1 ± 1.28	0.35	730

Chapter 6

Cosmology: Constructing the Hubble Diagram

6.1 Introduction

In addition to studying the physics of quasars by finding the relation between the disk UV and corona X-ray luminosities which was discussed in the previous chapters, the strength of the quasars' luminosities allows us to observe these objects up to redshifts of 7 (Mortlock et al., 2011). That means we have, more or less, new cosmological probes for measuring cosmic distances which we call "standard candles", just like Cepheids and SN1a[1].

In order to dive in the cosmological science of quasars, I will be performing two steps in the following Chapter. In section 2, luminosity distances (D_L) will be calculated, and those will be used in section 3 to build a Hubble Diagram and probe the cosmological models.

6.2 Calculating Luminosity Distances

Now it's important to deduce cosmic distances with the help of the extraordinary strength of quasars' luminosities.

What is a Luminosity Distance D_L?
Assume you are observing a far away galaxy at some given redshift z. In astronomy, we can know the distance of an object once we know the amount of photons received (also known as flux) using simple equations $F = \frac{L}{4\pi d^2}$, of course if we're able to calculate the luminosity, but not forgetting that this galaxy is attenuated by two important factors: **relativistic redshift** and **doppler redshift of emission**. Those two contribute to a factor of **(1+z)**^{2} each, thus leaving us with luminosity:

---

[1]By the help of Cepheids we were able to calculate distances within our Galaxy and SuperNovae 1a, SN1a, gave distances up to 1.5 redshift with high accuracy

[2]$(1 + z) = \frac{\lambda_{obs}}{\lambda_{emitted}}$

$$L_o = \frac{L_e}{(1+z)^2}$$

with L_o being the observed luminosity and L_e being the emitted luminosity.

Doppler redshift

Since galaxies and stars are moving away from us during observation, the light is shifted by a factor of (1+z)

Relativistic redshift

As photons move from the source objects towards us, it loses energy on its way, thus adding the (1+z) factor

Now in order to calculate D_L, first i will find the calculated values of the 2500Å luminosity. For this purpose, the $\alpha_{ox} - L_{2500\text{Å}}$ relation is used.

6.2.1 $\alpha_{ox} - L_{2500\text{Å}}$ Relation

Tananbaum et al. defined the relative ratio of optical-UV to X-ray fluxes. This should be understood as nothing but a simple parametrization of these two fluxes, and is not a true fit to the spectrum. This ratio is defined by a spectral index α_{ox}, given by:

$$\alpha_{ox} = -\frac{\log\frac{F_v(2keV)}{F_v(2500\text{Å})}}{\log\frac{v(2keV)}{v(2500\text{Å})}} = -0.384 \log \frac{F_v(2keV)}{F_v(2500\text{Å})} \tag{6.1}$$

Another way to describe the $logL_X - logL_{UV}$ relation is the use of a spectral index. A quick reminder that this relation showed that more optically luminous AGN are less luminous in X-rays. Following the same concept, the following has been plotted:

$$\alpha_{ox} = \gamma_1 L_{2500\text{Å}} + \beta_1 \tag{6.2}$$

In Fig 6.3,the spectral index as a function of the observed UV luminosity is shown. Given the values of α_{ox}, one can calculate $L_{2500\text{Å}}$ of the best fit line, giving 'theoretical' UV luminosity values.

6.2.2   Luminosity Distance Calculation

Luminosity Distance D_L can be expressed in different ways. It is mainly defined in terms of the relationship between absolute magnitude M and apparent magnitude m given by:

$$M - m = 5 - 5 \log D_L \tag{6.3}$$

This gives a very good approximation within our Galaxy. But as we go farther into space, Equation (6.3) is affected by redshift, space-time curvature [3]. time dilation... Thus another way to express D_L is through **flux-luminosity relationship**, given by:

$$F = \frac{L}{4\pi D_L^2} \tag{6.4}$$

Equation (6.4), thus, is a good approximation for D_L for extra-galactic objects like quasars, as we have taken into consideration the terms that affect luminosity, keeping it, more or less, unbiased.

In this study, the luminosity and flux used to calculate D_L are those corresponding to $2500\mathring{A}$[4]. Previously in this section, I've calculated the "theoretical" values for the $L_{2500\mathring{A}}$ from $\alpha_{ox} - L_{2500\mathring{A}}$ relation. Finally, D_L is computed following equation 6.4

6.2.3 Redshift Intervals

After plotting the $\log F_X$-$\log F_{UV}$ relation, the sample is divided into redshift bins to check the redshift dependence of this relation. This needs two requirements: (a) the scatter due to the different luminosity distances within each bin is small compared with the intrinsic dispersion and (b) each bin is sufficiently populated for a meaningful check. The analysis is performed for equally spaced bins with $\triangle \log z \leq 0.1$ (Lusso & Risaliti, 2017) to satisfy the first condition, and second condition is satisfied when taking redshift values starting at that which will have a reasonably populated sample.

For the condition given, $\triangle \log z \leq 0.1$, the number of bins achieved is 18, but the first 6 bins were neglected up to redshift z=0.28 since they are not populated enough to account for in a linear regression. The sample is divided into 12 bins following the work of (Lusso & Risaliti, 2017), and for each $< z >$ I plotted each interval of fluxes and performed a linear fit of the $\log F_X$ - $\log F_{UV}$ relation.

It is clear from the results shown in figures 6.4 & 6.5 that the slope, more or less, doesn't evolve with redshift and has an average value $\gamma = 0.638$ plotted in Fig. 6.2. This is an important note - the ratio of $\log F_X$ to $\log F_{UV}$ doesn't change when moving to higher redshifts and reassures us that there is some physical relation between the disk and the corona of the AGN independent of the distance to it.

---

[3]Discussed in section 6.3.2

[4]The reason for using 2500A luminosities is due to the high significance between α_{ox} and $L_{2500\mathring{A}}$ (Steffen et al., 2006). In addition to that, we were able to reduce host galaxy contamination and reddening at this wavelength.
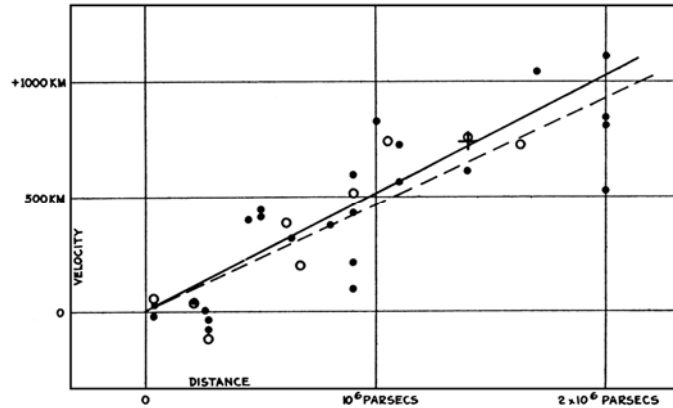
Figure 6.1: The original Hubble Diagram showing the peculiar velocity of extra galactic nebulae as a function of their distances. From this figure, one concludes that everything is moving away from us, and as it gets further it also moves faster away.

6.3   Constructing the Hubble Diagram

In this section I will finalize the results of this study.   From section 5.2, I calculated the luminosity distance of the 730 quasar sample. Using these results, I will build the Hubble Diagram and shed lights on how it can help us understand about the nature of Dark Energy (DE).

6.3.1   What is the Hubble Diagram

Briefly, a Hubble Diagram is the "plot" of Hubble's Law, where one plots the velocity as a function of distance of the source object given by the linear law:

$$v = H_0 d$$

where H_0 is the Hubble constant and $\frac{1}{H_0}$ is the Hubble time.

History

In 1929, Edwin Hubble released his article "A relation between distance and radial velocity among extra-galactic nebulae"(Hubble, 1929). He widened our understanding of the universe we live in, making a revolution in the 20th century. Hubble reported that the Universe is expanding, that means, observing distant galaxies, we notice that they are moving away from us in all directions. And when looking at farther objects, we notice that they're moving at higher speeds.

A very important note concerning Hubble's Law: it only works on distant galaxies. As for nearby galaxies in the Local Group and stars within our Galaxy, the peculiar velocity (note: motion of objects within the Galaxy about its center) is much higher than the recession velocity.

6.3.2 ΛCDM Model

The ΛCDM Model (Λ stands for Dark Energy with constant energy density and CDM for cold dark matter) is favored by observational cosmologists. It is a model that assumes the universe is spatially flat, thus Euclidean geometry can be used, its expansion is not affected by curvature, and Newtonian mechanics can be applied locally[5].

In this study, a ΛCDM model is assumed with the latest Hubble constant value $H_0 = 67.8$ kms^{-1}Mpc^{-1}, and the estimated cosmology parameters $\Omega_M = 0.28$ and $\Omega_\Lambda = 0.72$ (Komatsu et al., 2009), Ω_Λ being the fraction of the total energy density and Ω_M being the mass density including ordinary mass (baryonic and dark matter). The results of luminosity distance previously calculated in section 6.2.2 are now plotted as a function of redshift z in figure 6.3.2

---

[5]by locally we mean it can be extended to cosmological scales and extragalactic distances
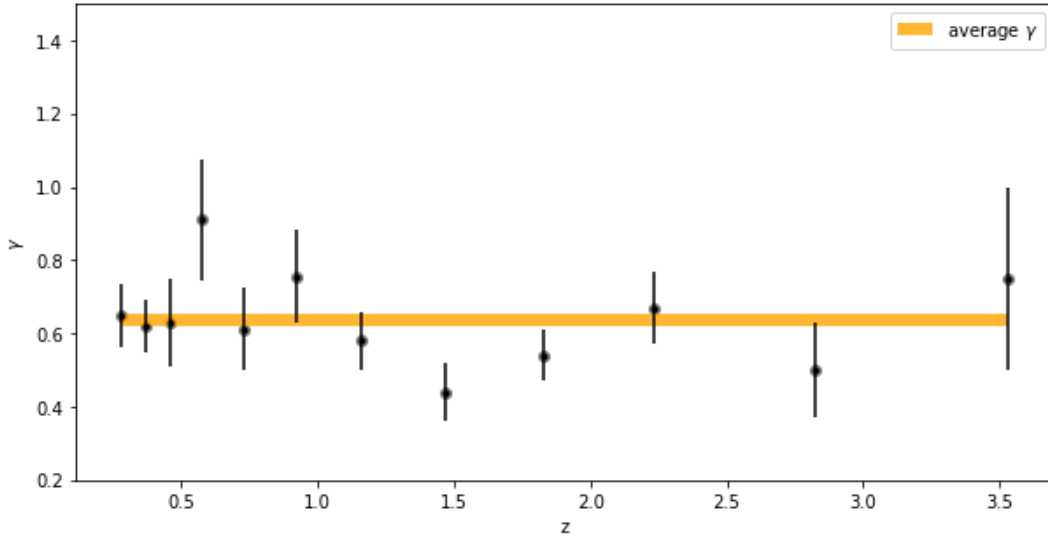
Figure 6.2: Slope evolution of the binned sample with error bars and an average value $\gamma = 0.638$
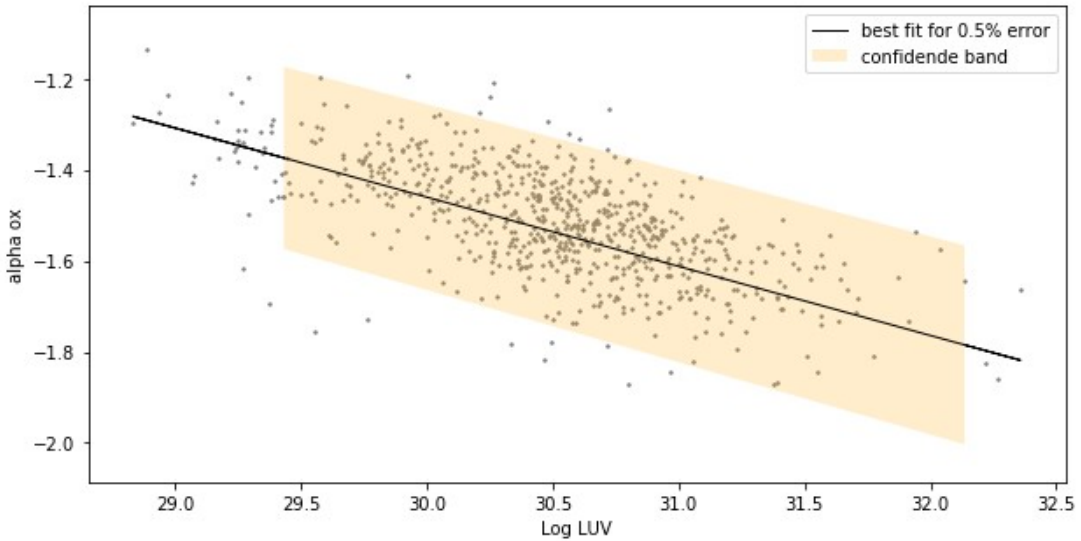
Figure 6.3: α_{ox} - $\log L_{2500\mathring{A}}$ plot of 730 obtained objects. The following relation is a by-product of the $\log L_X - \log L_{UV}$ relation showing an anti-correlation between α_{ox} and the luminosity at $2500\mathring{A}$.
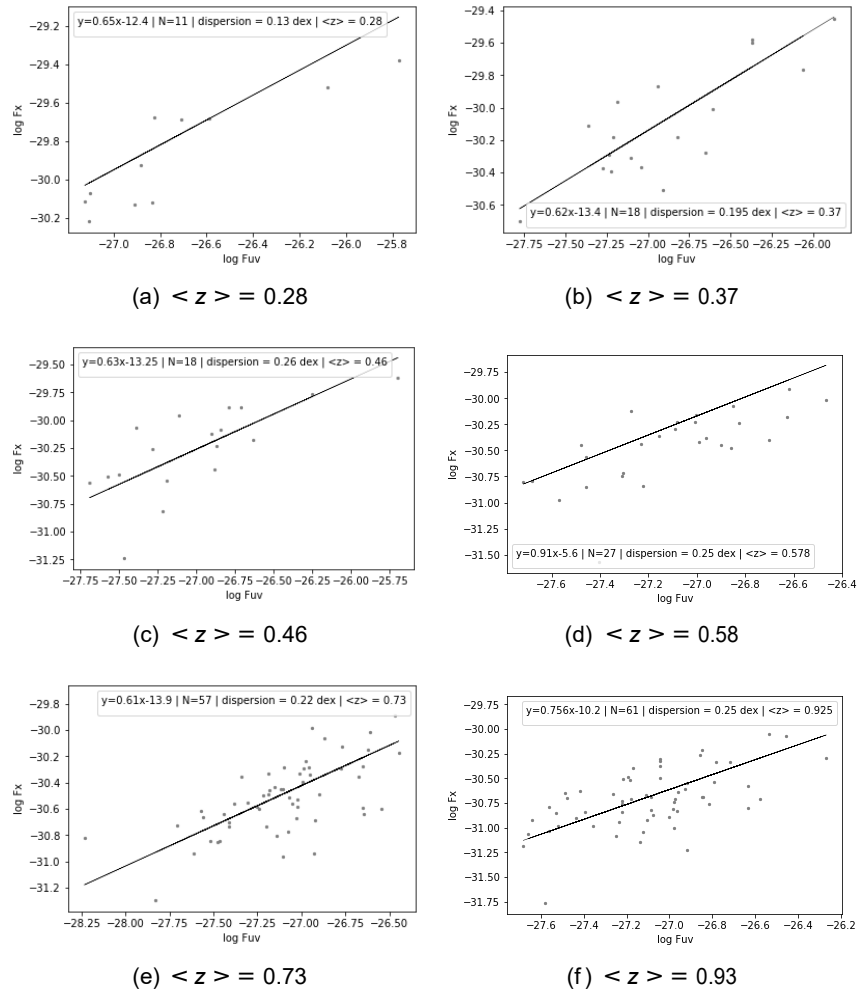
(a) $<z> = 0.28$

(b) $<z> = 0.37$

(c) $<z> = 0.46$

(d) $<z> = 0.58$

(e) $<z> = 0.73$

(f) $<z> = 0.93$

Figure 6.4: $logF_X - logF_{UV}$ relation subplots of each bin

(a) $< z > = 1.2$

(b) $< z > = 1.46$

(c) $< z > = 1.83$

(d) $< z > = 2.23$

(e) $< z > = 2.8$

(f) $< z > = 3.5$

Figure 6.5: $logF_X - logF_{UV}$ relation subplots of each bin (continued)

Figure 6.6: Hubble Diagram of the sample achieved in this study of 730 quasars. Grey dots being the full sample plotted, the black dots are the redshift bins of the previously assorted quasars and the yellow line is the ΛCDM model fit assuming the parameters: $H_0 = 67.8 kms^{-1} Mpc^{-1}$, $\Omega_M = 0.28 \pm 0.04$ and $\Omega_\Lambda = 0.72$

Chapter 7

Discussion and Conclusion

7.1 Summary and Conclusion

The physical relation between X-ray and UV fluxes

The aim of this thesis work has been to restudy the main sample delivered by (Lusso & Risaliti, 2016) in order to plot the physical properties in a log-log plot to achieve a linear relation with the least dispersion possible in order to better understand the physical mechanism that might be happening in the AGN's disk-corona system. The relations were plotted using fluxes ($\log F_X - \log F_{UV}$) and luminosities ($\log L_X - \log L_{UV}$) using a statistical method presented by (Akritas & Bershady, 1996) that was modified in o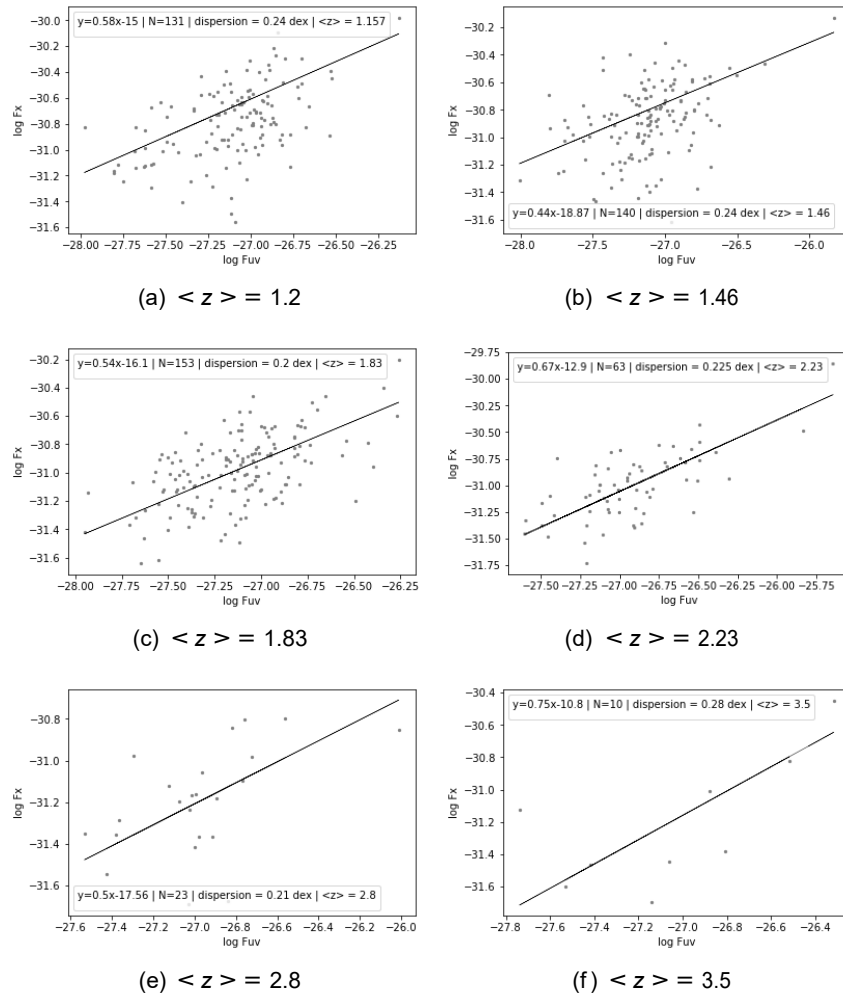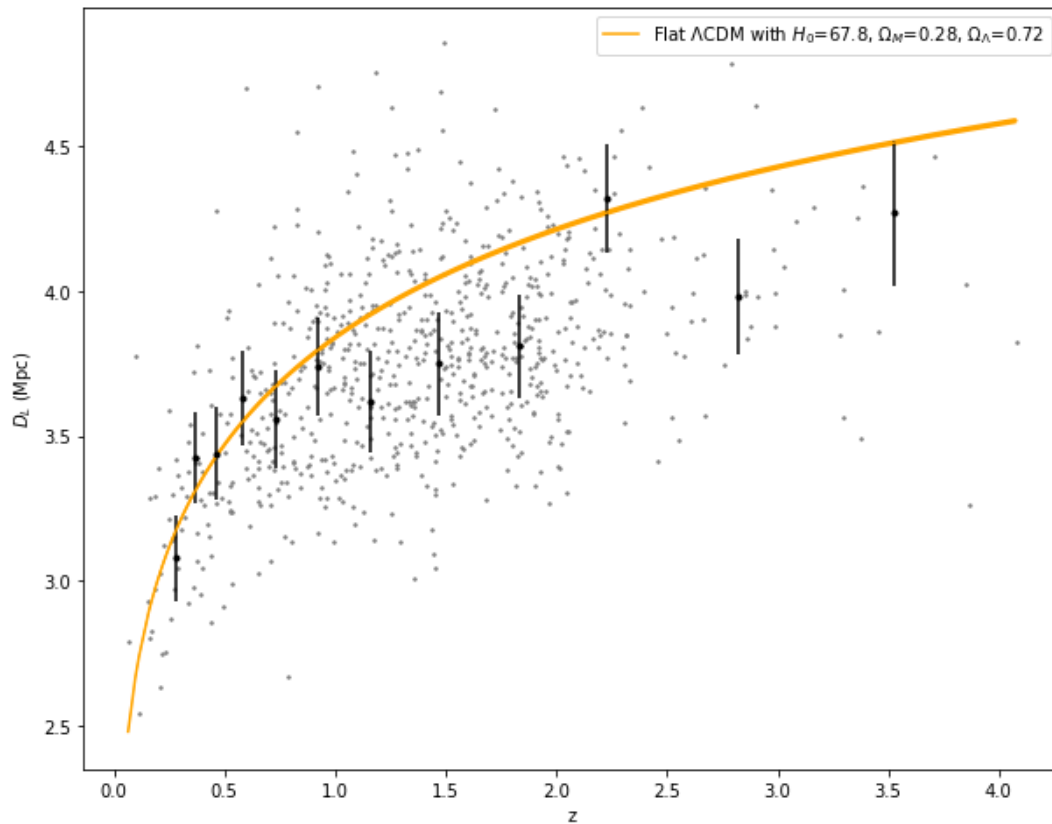rder to estimate the intrinsic dispersion. Where the presented frequencies are those of the accretion disk (emitting at 2500 A) close to the bulge of the BH and that of the corona that emits in X-ray. The predicted mechanism has been previously mentioned by (Lusso & Risaliti, 2016) that there is inverse Compton up-scattering of the photons from the accretion disk onto the corona which gives rise to the X-ray radiation. Yet the excess dispersion not yet well understood ($\sim$ 0.21-0.24) apart from the fact that the fluxes exhibit variability on the scale of weeks/year that contributes to 31% of the dispersion (0.12 dex). As for the rest of the dispersion, it remains an open question.

The intrinsic dispersion gave interesting results in the $\log L_X - \log L_{UV}$ relation ($\delta_{int} \sim 0.23 - 0.24$ dex), very similar to that of (Lusso & Risaliti, 2016). But when this relation was restudied for $\log F_X - \log F_{UV}$, the dispersion was high again reaching 0.35-0.36 dex[1]. Another interesting observation was made when the fluxes were divided into redshift bins, the intrinsic dispersion dropped significantly reaching an average value of 0.22 dex. Again, it is important to perform this study using fluxes instead of luminosities which are cosmology dependent leaving us with extra biases and focus on adjusting the sample based on the study of quasars' flux.

Using quasars as cosmological probes

As for the second part of this work, since quasars are good cosmological probes, their

---

[1] According to (Lusso & Risaliti, 2016), the real physical intrinsic dispersion should be < 0.21 dex after eliminating measurement uncertainties and variability

physical properties can give really good approximations of distances in the universe up to redshifts 7. In this work, we have presented the Hubble Diagram of quasars up to redshifts ~4 which was shown in fig 6.3.2. For this, we have used the by-product of the log-log plot of luminosities - the $\alpha_{OX} - \log L_{UV}$. From the following relation, we could estimate the *theoretical* $L_{2500\text{Å}}$ which were then used to estimate luminosity distances of each quasar.

The final product of this study was plotting the Hubble Diagram of luminosity distances as a function of redshift z. The plot showed acceptable results within uncertainties attained with the most recent Hubble constant value $H_0 = 70\ kms^{-1}Mpc^{-1}$ and estimated cosmological parameters $\Omega_M = 0.28 \pm 0.04$ and $\Omega_\Lambda = 0.72$.

7.2   Future Prospects

The first step of this study has been covered throughout this thesis. The next step is to constrain the Dark Energy Equation of State by estimating the simple first order linear expansion of this equation: $\omega(z) = \omega(0) + \omega_z z$ and later the FLRW cosmology with a CPL (Chevallier-Polarski-Linder) dark energy equation of state and curvature: $\omega(z) = \omega(0) + \omega_a(1 - a) = \omega(0) + \omega_a z/(1 + z)$.

Another important thing to do is trying to get rid of cosmology dependence during the study, and that's why it's better to perform the work using fluxes instead of luminosities (which are directly dependent on cosmological model). But, as mentioned the intrinsic dispersion of fluxes stayed high (~ 0.34 dex), although when dividing the quasars into smaller bins, the intrinsic dispersion dropped significantly reaching an average value of $\delta_{int} \sim 0.22$ dex. This matter should be resolved by further studying what factors are affecting this high value of dispersion even after cleaning host galaxy contamination and reddening. Also, address intrinsic dispersion of small redshift bins and answer the question: why is the dispersion high in the full sample while it's dropping when the sample is dissected?

In addition to that, we should address the matter of variability of flux in AGN, better understand why does this phenomenon occurs and how does it affect the other physical mechanisms that might also occur in the disk and corona.

The proposed solution for this is to work with each bin and perform the cleaning accordingly to each bin. Only then, one can estimate luminosity distances, estimate cosmological parameters and better constrain the Dark Energy Equation of State (EOS). As a result, the Hubble Diagram would be built piece by piece.

References

Akritas, M. G., & Bershady, M. A. (1996). Linear regression for astronomical data with measurement errors and intrinsic scatter. *arXiv preprint astro-ph/9605002*.

Avni, Y., Soltan, A., Tananbaum, H., & Zamorani, G. (1980). A method for determining luminosity functions incorporating both flux measurements and flux upper limits, with applications to the average x-ray to optical luminosity ratio for quasars. *The Astrophysical Journal*, *238*, 800–807.

Avni, Y., & Tananbaum, H. (1982). On the cosmological evolution of the x-ray emission from quasars. *The Astrophysical Journal*, *262*, L17–L21.

Baldwin, J. A. (1977). Luminosity indicators in the spectra of quasi-stellar objects. *The Astrophysical Journal*, *214*, 679–684.

Betoule, M. e. a., Kessler, R., Guy, J., Mosher, J., Hardin, D., Biswas, R., . . . others (2014). Improved cosmological constraints from a joint analysis of the sdss-ii and snls supernova samples. *Astronomy & Astrophysics*, *568*, A22.

Bisogni, S., Risaliti, G., & Lusso, E. (2018). A hubble diagram for quasars. *Frontiers in Astronomy and Space Sciences*, *4*, 68.

Brandt, W., Laor, A., & Wills, B. J. (2000). On the nature of soft x-ray weak quasi-stellar objects. *The Astrophysical Journal*, *528*(2), 637.

Dai, D.-C., Starkman, G. D., Stojkovic, B., Stojkovic, D., & Weltman, A. (2012). Using quasars as standard clocks for measuring cosmological redshift. *Physical review letters*, *108*(23), 231302.

Eddington, A. (1913). On a formula for correcting statistics for the effects of a known error of observation. *Monthly Notices of the Royal Astronomical Society*, *73*, 359–360.

Gallagher, S., Brandt, W., Sambruna, R., Mathur, S., & Yamasaki, N. (1999). Exploratory asca observations of broad absorption line quasi-stellar objects. *The Astrophysical Journal*, *519*(2), 549.

Gibson, R. R., Jiang, L., Brandt, W., Hall, P. B., Shen, Y., Wu, J., . . . others (2009). A catalog of broad absorption line quasars in sloan digital sky survey data release 5. *The Astrophysical Journal*, *692*(1), 758.

Green, P. J., & Mathur, S. (1995). Broad absorption line qsos observed by the rosat pspc. *arXiv preprint astro-ph/9512032*.

Hubble, E. (1929). A relation between distance and radial velocity among extra-galactic nebulae. *Proceedings of the National Academy of Sciences*, *15*(3), 168–173.

Kellermann, K., Sramek, R., Schmidt, M., Shaffer, D., & Green, R. (1989). Vla observations of objects in the palomar bright quasar survey. *The Astronomical Journal*, *98*, 1195–1207.

Kelly, B. C. (2007). Some aspects of measurement error in linear regression of astronomical data. *The Astrophysical Journal*, *665*(2), 1489.

Komatsu, E., Dunkley, J., Nolta, M., Bennett, C., Gold, B., Hinshaw, G., . . . others (2009). Five-year wilkinson microwave anisotropy probe* observations: cosmological interpretation. *The Astrophysical Journal Supplement Series*, *180*(2), 330.

La Franca, F., Bianchi, S., Ponti, G., Branchini, E., & Matt, G. (2014). A new cosmological distance measure using active galactic nucleus x-ray variability. *The Astrophysical Journal Letters*, *787*(1), L12.

Lusso, E., Comastri, A., Vignali, C., Zamorani, G., Brusa, M., Gilli, R., . . . others (2010). The x-ray to optical-uv luminosity ratio of x-ray selected type 1 agn in xmm-cosmos. *Astronomy & Astrophysics*, *512*, A34.

Lusso, E., & Risaliti, G. (2016). The tight relation between x-ray and ultraviolet luminosity of quasars. *The Astrophysical Journal*, *819*(2), 154.

Lusso, E., & Risaliti, G. (2017). Quasars as standard candles-i. the physical relation between disc and coronal emission. *Astronomy & Astrophysics*, *602*, A79.

Mortlock, D. J., Warren, S. J., Venemans, B. P., Patel, M., Hewett, P. C., McMahon, R. G., . . . others (2011). A luminous quasar at a redshift of z= 7.085. *Nature*, *474*(7353), 616.

Nemmen, R. S., Georganopoulos, M., Guiriec, S., Meyer, E. T., Gehrels, N., & Sambruna, R. M. (2012, December). A Universal Scaling for the Energetics of Relativistic Jets from Black Hole Systems. *Science*, *338*, 1445. doi: 10.1126/science.1227416

Peterson, B. M. (1997). *An introduction to active galactic nuclei*. Cambridge University Press.

Peterson, B. M., & Horne, K. (2006). Reverberation mapping of active galactic nuclei. In *Planets to cosmology: Essential science in the final years of the hubble space telescope* (Vol. 18, p. 89).

Riess, A. G., Filippenko, A. V., Challis, P., Clocchiatti, A., Diercks, A., Garnavich, P. M., . . . others (1998). Observational evidence from supernovae for an accelerating universe and a cosmological constant. *The Astronomical Journal*, *116*(3), 1009.

Risaliti, G., & Lusso, E. (2015). A hubble diagram for quasars. *The Astrophysical Journal*, *815*(1), 33.

Rosen, S., Webb, N., Watson, M., Ballet, J., Barret, D., Braito, V., . . . others (2016). The xmm-newton serendipitous survey-vii. the third xmm-newton serendipitous source catalogue. *Astronomy & Astrophysics*, *590*, A1.

Sabra, B. M., Saliba, C., Akl, M. A., & Chahine, G. (2015). The black hole–dark matter halo connection. *The Astrophysical Journal*, *803*(1), 5.

Schmidt, M. (1990). *The discovery of quasars*. Cambridge, UK: Cambridge University Press.

Shen, Y., Richards, G. T., Strauss, M. A., Hall, P. B., Schneider, D. P., Snedden, S., . . . others (2011). A catalog of quasar properties from sloan digital sky survey data release 7. *The Astrophysical Journal Supplement Series*, *194*(2), 45.

Steffen, A. T., Strateva, I., Brandt, W., Alexander, D., Koekemoer, A., Lehmer, B., . . . Vignali, C. (2006). The x-ray-to-optical properties of optically selected active galaxies over wide luminosity and redshift ranges. *The Astronomical Journal*, *131*(6), 2826.

Tananbaum, H., Avni, Y., Branduardi, G., Elvis, M., Fabbiano, G., Feigelson, E., . . . others (1979). X-ray studies of quasars with the einstein observatory. *The Astrophysical Journal*, *234*, L9–L13.

Taylor, M. B. (2005). Topcat & stil: Starlink table/votable processing software. In *Astronomical data analysis software and systems xiv* (Vol. 347, p. 29).

Tremaine, S., Gebhardt, K., Bender, R., Bower, G., Dressler, A., Faber, S. M., . . . others (2002). The slope of the black hole mass versus velocity dispersion correlation. *The Astrophysical Journal*, *574*(2), 740.

Urry, C. M., & Padovani, P. (1995). Unified schemes for radio-loud active galactic nuclei. *Publications of the Astronomical Society of the Pacific*, *107*(715), 803.

Watson, D., Denney, K., Vestergaard, M., & Davis, T. M. (2011). A new cosmological distance measure using active galactic nuclei. *The Astrophysical Journal Letters*, *740*(2), L49.

Zeldovich, Y. B., & Novikov, I. (1964). Relativistic astrophysics. part i. *Uspekhi Fizicheskikh Nauk (USSR) For English translation of v61 1957-v65 1958 see Advan. Phys. Sci.(USSR)*, *84*.

Appendices

Appendix A

Intrinsic Scatter Explained with example

For a better understanding of what intrinsic scatter is, I will provide a simple example. Going back to high school physics, assume you have to calculate the resistance using Ohm's law in an experiment having circuits providing the voltage U and current I. But we will have two different cases here:

Case 1:

In this case, there will be one circuit, and we will take 10 measurements of the current upon changing the voltage. Plotting the results, the resistance R will be the slope. The uncertainty in this case is the measurement uncertainty due to the measuring instruments.

Case 2:

Now, we will take 10 different circuits with the same properties and take 1 measurement from each. Again plot the voltage across current. The uncertainty here is due to 2 factors:

1. Measurement uncertainty due to the instruments measuring the voltage and current

2. Additional uncertainty since each circuit has different material (even having the same properties, for example the connecting wires aren't a 100% the same). This contributes to a slight shift in the values due to the nature of the circuit, what is called 'intrinsic scatter'.